Comparison of Electron-Transfer and Charge-Retention Characteristics of Porphyrin-Containing Self-Assembled Monolayers Designed for Molecular Information Storage

Kristian M. Roth,[†] Daniel T. Gryko,[‡] Christian Clausen,[‡] Junzhong Li,[‡] Jonathan S. Lindsey,*[,‡] Werner G. Kuhr,*[,†] and David F. Bocian*[,†]

Department of Chemistry, University of California, Riverside, California 92521-0403, and Department of Chemistry, North Carolina State University, Raleigh, North Carolina 27695-8204

Received: March 28, 2002; In Final Form: June 11, 2002

The redox kinetics for a variety of porphyrin-containing self-assembled monolayers (SAMs) on Au are reported. The measurements probe both the rate of electron-transfer (k^0) for oxidation (in the presence of applied potential) and the rate of charge dissipation after the applied potential is disconnected (characterized by a charge-retention half-life ($t_{1/2}$)). The porphyrins include (1) monomeric Zn complexes that contain phenylmethylene linkers wherein the number of methylene spacers varies from 0 to 3, (2) monomeric Zn complexes that contain different ethynylphenyl-derived linkers, and (3) a triple-decker lanthanide sandwich complex with a phenylethynylphenyl linker. The k^0 values for all the porphyrin SAMs are in the range of 10^4-10^5 s^{-1}. The k^0 values for the monomeric ethynylphenyl-linked porphyrin SAMs are generally faster than those for the monomeric phenylmethylene-linked SAMs. The rates for the latter SAMs decrease as the number of methylene spacers increases. The rates for the triple-decker SAM are generally slower than those for the monomers. The trends observed in the k^0 values are paralleled in the $t_{1/2}$ values, that is, porphyrin SAMs that exhibit relatively faster electron-transfer rates also exhibit faster charge-dissipation rates (shorter $t_{1/2}$ values). However, the charge-dissipation rates (no applied potential) are approximately 6 orders of magnitude slower than the electron-transfer rates (applied potential). Both the k^0 and $t_{1/2}$ values for the porphyrin SAMs are sensitive to the surface coverage of the molecules. The rates for both processes decrease as the monolayers become more densely packed. This behavior is attributed to exclusion of solvent/counterions and space-charge effects. The effect of surface coverage on rates can overshadow differences that result from differences in linker type/length. Collectively, the studies help to delineate the molecular design features that could be manipulated to control the redox processes in porphyrin SAMs. The understanding of these processes is essential for the successful implementation of molecules as the active media in information-storage elements.

Introduction

We have been engaged in a program aimed at constructing devices that use the properties of molecules to store information.[1−4] In our general approach, a collection of redox-active molecules in a self-assembled monolayer (SAM) attached to an electroactive surface serves as the active storage medium. Our studies have focused primarily on porphyrin-based architectures. During these studies, a library of 100+ molecules has been prepared and characterized.[5−10] The generic architecture consists of a redox-active molecule, a linker, and a surface attachment group. In most cases, the surface attachment group has been a thiol for binding to an Au surface. The redox-active molecules span several classes including (1) monomeric porphyrins,[5] (2) ferrocene porphyrins,[6] (3) weakly coupled multimeric porphyrins,[7] (4) tightly coupled multimeric porphyrins,[8] (5) triple-deckers of lanthanide porphyrins and phthalocyanines,[3,9] and more recently, (6) covalently linked dyads of triple deckers.[10] The primary goals for examining the more complex architectures were (1) to increase the number of available oxidation states, thereby increasing the information storage density and (2) to achieve very low redox potentials, thereby affording lower power consumption in an actual device. Molecules with a variety of linkers have also been examined.[1,2,5] The goal of these studies was to determine how linker length and composition affect the duration of charge storage (i.e., charge retention) in the SAM after disconnection from the source of applied potential. Long charge-retention times are extremely desirable for most memory applications.

A subset of the porphyrin molecules that we have examined for information storage purposes is shown in Figure 1. These molecules include (1) a series with phenylmethylene linkers, designated **PMn** (n = 0−3), (2) a group with ethynylphenyl linkers, designated **EP**, **PEP**, and **PEPM**, and (3) a triple decker with a phenylethynylphenyl linker, designated **TD**. A noteworthy design feature of each of these molecules is that the nonlinking substituent groups (mesityl, phenyl, *p*-tolyl) of the porphyrins are bulky and relatively nonpolar. This feature is essential for achieving good solubility in the organic solvents from which the porphyrins are deposited to form the SAMs. The bulky, nonpolar substituents also serve a second important function, in particular, to attenuate electronic interactions between adjacent porphyrins in the SAMs. This "self-insulating" feature of the porphyrins precludes the need for diluting the redox-active molecules with nonredox active coadsorbates (as

* To whom correspondence should be addressed.
[†] University of California.
[‡] North Carolina State University.

10.1021/jp025850a CCC: $22.00
Published on Web 08/03/2002

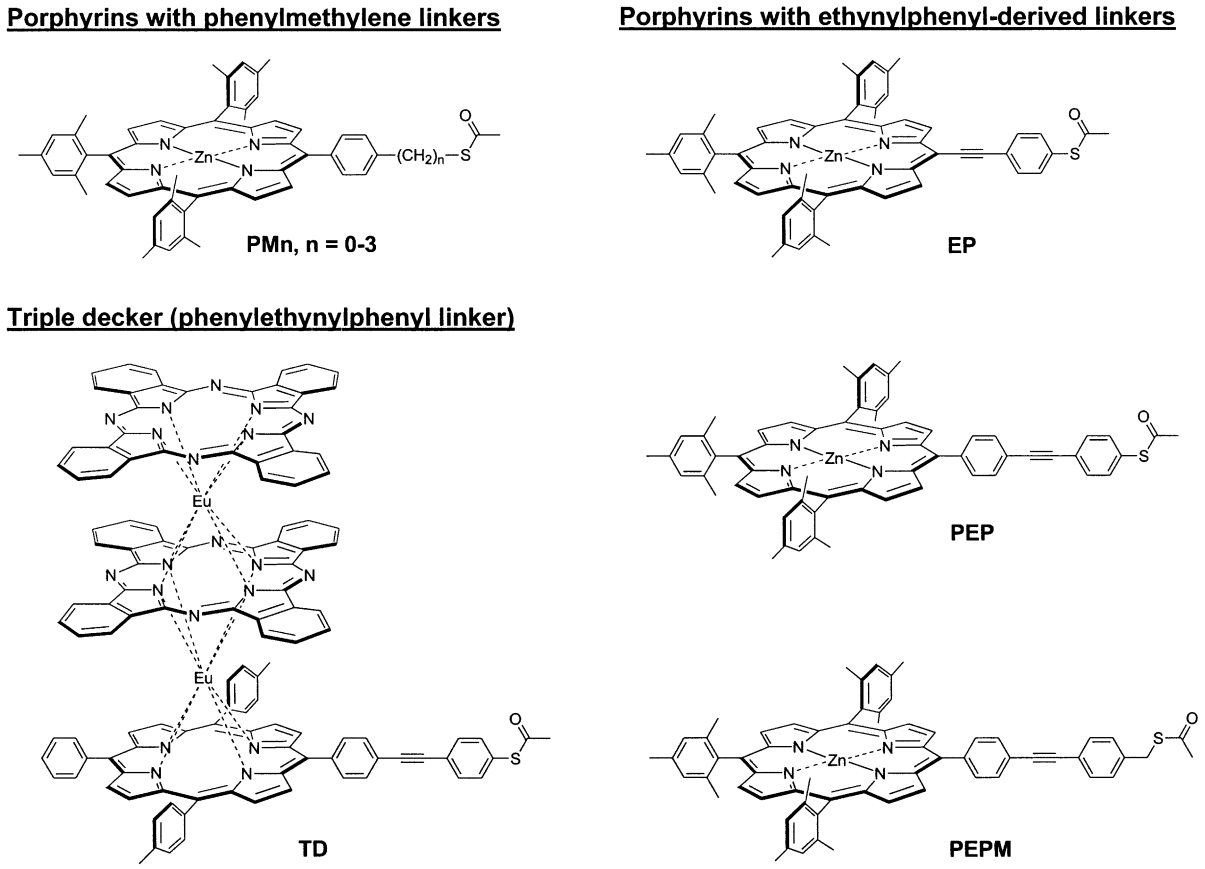

Figure 1. Molecules for preparing the SAMs. The *S*-acetyl protecting group undergoes facile cleavage upon exposure to the Au surface.[1−10,30]

is typically done to suppress electronic interactions in SAMs containing thiol-derivatized alkylferrocenes). Eliminating the use of diluents affords a higher surface density of redox-active species, which is generally desirable from a device standpoint because more charge can be stored per unit area, thereby enabling the use of smaller feature sizes for memory storage elements.

Our previous studies of SAMs of the porphyrins shown in Figure 1 indicate that each of these molecules is capable of retaining charge for extended periods.[1−3] The kinetics of charge dissipation are approximately first-order; accordingly, we have found it convenient to characterize the charge-retention characteristics of the SAMs in terms of a half-life ($t_{1/2}$). The $t_{1/2}$ values for SAMs of the porphyrins shown in Figure 1 range from tens of seconds to tens of minutes, depending on the specific architecture. The phenylmethylene-linked porphyrin SAMs generally exhibit the longest charge-retention times. These times monotonically increase as the number of methylene spacers increases ($t_{1/2} \sim$ 120, 170, 660, and 890 s for n = 0−3, respectively).[1] The ethynylphenyl-linked porphyrin SAMs exhibit generally shorter charge-retention times.[2] These times also increase monotonically as the length of the linker increases ($t_{1/2} \sim$ 30, 40, and 60 s for **EP**, **PEP**, and **PEPM,** respectively). The charge-retention times of the **TD** SAM (which also contains a phenylethynylphenyl linker) are generally similar to those of the SAMs of the ethynylphenyl-linked porphyrin monomers.[3] In addition, the charge-retention times of the **TD** SAM monotonically increase as the oxidation state increases ($t_{1/2} \sim$ 15, 30, 60, and 75 s for the mono-, di-, tri-, and tetracations, respectively).

The trends in the charge-retention characteristics of the porphyrin SAMs are qualitatively consistent with the observations of other studies of electron transfer in redox-active SAMs. In particular, (1) nonconjugated linkers generally yield slower rates than conjugated linkers and (2) the addition of methylene spacers to the linker slows the rates.[11−23] In the **TD** SAM, the longer charge-retention times for the higher oxidation states are consistent with a charge-dissipation pathway wherein each oxidation state of a given molecule in the SAM decays sequentially to the next lower one until the molecule is neutral.[3] For all the porphyrin SAMs, the mechanism of charge dissipation is thought to be the recombination of Au conduction-band electrons with the porphyrin holes (rather than, for example, electron injection from the solvent/electrolyte).[4] This process is slow under conditions of no applied potential, leading to relatively long charge-retention times for all the porphyrin SAMs.

An important parameter relating to the use of porphyrin SAMs as an information-storage medium is the rate of electron transfer under conditions of applied potential. This rate will be the ultimate determinant of the writing/erasing (and possibly reading) speed of a memory element. Our previous fast-scan voltammetric studies of porphyrin SAMs on microelectrodes have shown that these rates are much faster than the charge-dissipation rates under conditions of no applied potential.[1−10] However, these measurements did not provide a quantitative value for the electron-transfer rate. In the present study, we have measured the electron-transfer rates of SAMs prepared from the molecules shown in Figure 1. The objective of this work is not to examine electron-transfer rates per se but rather to determine how the electron-transfer rates (applied potential) correlate with charge-dissipation rates (no applied potential) and how both of these rates are affected by the surface concentration of the electroactive molecules. The electron-transfer rates were measured by using a ratiometric AC voltammetric technique recently introduced by Creager and co-workers for measuring

the electron-transfer kinetics of redox-active SAMs.[21,24−28] This method enjoys the advantage that the data analysis is much more straightforward than that required for other methods typically used to measure the redox kinetics of SAMs. During our work, we introduced a modification to the ratiometric method that affords multiplex-advantaged data acquisition, thereby enhancing the general utility of the method. Collectively, the studies reported herein provide new insights into the factors that control the electron-transfer and charge-retention characteristics of porphyrin SAMs.

Experimental Section

Chemicals and Materials. CH_2Cl_2 (Aldrich), propylene carbonate (Aldrich), absolute ethanol (Gold Seal), $HClO_4$ (Aldrich, 70%), and $CH_3(CH_2)_{11}SH$ (Aldrich) were used as received. Bu_4NPF_6 (Aldrich) and Bu_4NClO_4 (Kodak) were triply recrystallized from methanol and ethanol, respectively, and dried in vacuo at 110 °C before use. **PMn** (n = 0−3), **EP**, **PEP**, **PEPM**, and **TD** were synthesized as *S*-acetylthio derivatives as previously described.[3,5,9] $Fc(CH_2)_{12}SAc$ was prepared following the approach outlined by Chidsey et al. for an homologous compound.[29] The *S*-acetyl protecting group undergoes facile cleavage upon exposure to the Au surface.[1−10,30]

Electrode Preparation. The electrochemical measurements on the SAMs were made using Au ball working electrodes prepared from Au wire (Goodfellow, >99.99% pure) sealed in soft glass. The diameter of the wire was either 5 or 250 μm, depending on the size of the electrode desired (vide infra). For the electrodes prepared from the 5-μm diameter wire, an ∼500-μm length segment of the wire was initially protruding from the end of 1-mm i.d. soft glass tubing; for the electrodes prepared from the 250-μm diameter wire, the end of the wire was initially nearly flush with the end of the glass tubing. Exposure of the electrode to a flame causes the wire to melt into a ball that terminates at the surface of the glass, which forms a tight seal around the Au. After flame exposure, the electrodes were cooled in a stream of nitrogen and used immediately.

The porphyrin SAMs were studied only on the electrodes prepared from the 5-μm diameter wire. The average electrochemical area of these electrodes was $\sim 1.5 \times 10^{-5}$ cm^2 (determined by using cyclic voltammetry and a standard ferrocene solution).[31] The RC time constant of the electrochemical cell (microelectrode/electrolyte) system was found to be ∼5 μs (as evaluated by using a potential step function). A relatively short cell time constant is essential for measuring the (relatively) fast electron-transfer kinetics of the porphyrin SAMs. The use of microelectrodes is also essential for performing the charge-retention measurements described below.[4]

The ferrocene SAMs (derived from $Fc(CH_2)_{12}SH$ and a coadsorbate, $CH_3(CH_2)_{11}SH$) were initially examined on the small electrodes (prepared from the 5-μm diameter wire). However, under the dilution conditions used to prepare the SAMs (vide infra), the currents were too low for reliable evaluation of the new voltammetric technique described herein. Consequently, the ferrocene SAMs were studied on the larger electrodes (prepared from the 250-μm diameter wire). The average electrochemical area of these electrodes was $\sim 4.5 \times 10^{-4}$ cm^2. The RC time constant for this electrochemical cell (∼150 μs) is too long to measure the electron-transfer kinetics of the porphyrin SAMs. However, it is sufficiently short to measure the much slower electron-transfer kinetics of the ferrocene SAMs.

Monolayer Preparation. The porphyrin SAMs were formed by placing the electrode in an ∼1 mM solution (in CH_2Cl_2) of the *S*-acetylthio-derivatized compound. The deposition time was varied to reach the desired SAM surface concentration and ranged from 15 s to 20 min. Upon removal from the sample solution, the electrode was rinsed with CH_2Cl_2 and used immediately. No diluents/coadsorbates were used in the preparation of the porphyrin SAMs. As was noted above, the bulky, nonpolar peripheral substituents on the porphyrin serve to electrically isolate the molecules from one another in the SAMs. The ability to prepare the porphyrin SAMs free of diluents/coadsorbates has important practical consequences. In particular, the use of diluents/coadsorbates compromises the quality of the porphyrin SAMs, as evidenced by extremely poor quality cyclic voltammograms relative to those exhibited by neat porphyrin SAMs (K. M. Roth, W. G. Kuhr, and D. F. Bocian, unpublished results). Even mild procedures, such as annealing the porphyrin SAMs in a vapor of alkanethiol, compromise the electrochemical response.

The ferrocene SAMs were prepared as a dilute, mixed monolayer of $Fc(CH_2)_{12}SH$ and the coadsorbate $CH_3(CH_2)_{11}SH$ in a 1:9 ratio. The deposition solution (absolute ethanol) was ∼1 mM in total thiol concentration. The details of the procedure used to form the ferrocene SAMs were made identical to those described in ref 27 to ensure that the redox kinetics measured by using the modified ratiometric method described herein could be reliably compared with those previously reported.

Electrochemical Measurements. Most of the electrochemical measurements on the porphyrin SAMs were performed in CH_2Cl_2 containing 1 M Bu_4NPF_6 as the supporting electrolyte. Selected data were also obtained using propylene carbonate/Bu_4NPF_6 or absolute ethanol/Bu_4NClO_4 as the solvent/electrolyte. A bare silver wire (Ag/Ag^+) served as the counter/reference electrode. The electrochemical measurements on the ferrocene SAMs were performed in 1 M $HClO_4$ using a Ag/AgCl reference electrode in saturated KCl. Cyclic voltammograms were recorded at 100 V s^{-1} with an in-house constructed potentiostat using a routine written in LabVIEW (National Instruments, Austin, TX).

Determination of Electron-Transfer Rates. The standard electron-transfer rate constants (k^0) of the porphyrin SAMs were measured using a variation of an AC voltammetric technique recently developed by Creager and co-workers for the purpose of measuring the redox kinetics of SAMs.[21,24−28] In the method of Creager and co-workers, AC voltammetric data are obtained at two different DC offset potentials: (1) the formal potential of the SAM and (2) a background potential that is well below the formal potential.[24,26] The current obtained at the formal potential (I_{peak}) is then ratioed to that obtained at the background potential (I_{bkgd}). The frequency of the small amplitude (10 mV) sine wave used in the AC voltammetric experiment is then varied, and a plot of I_{peak}/I_{bkgd} versus frequency is generated. At the background potential, no faradaic processes occur and the frequency response is solely a result of the electronic properties of the electrochemical cell, which include the solution resistance (R_{sol}) and the double-layer capacitance of the electrode surface (C_{dl}). At the formal potential, a faradaic current is present in addition to the background current, and the frequency dependence of the former process is convolved with the frequency dependence of the latter. The frequency response of the faradaic process is governed by the charge-transfer resistance (R_{ct}) and by the pseudocapacitance of the adsorbed monolayer (C_{ads}). Ratioing the current monitored at the formal potential to that observed at the background potential eliminates the background response. The k^0 values are then extracted from the

data by fitting I_{peak}/I_{bkgd} versus frequency to a Randles equivalent circuit model on the basis of the circuit elements R_{sol}, C_{dl}, R_{ct}, and C_{ads}. The modeling procedure will be described in more detail below.

In our experiment, the procedure of Creager and co-workers was modified in the following manner. Rather than obtaining data sets at several discrete frequencies, the frequency of the sinusoidal potential waveform was swept in time. The amplitude of the sine wave was held constant during this time sweep. The data generated in the swept-waveform voltammetric (SWAV) experiment was then Fourier transformed to obtain a conventional current-frequency plot. The applied waveform for the SWAV experiment was generated using the equation

$$y_i = A \times \sin((a/2i + b)i) \qquad i = 0, 1, 2, ..., n - 1 \quad (1)$$

where A is the amplitude of the applied waveform, $a = 2\pi(f_{end} - f_{begin})/n$ and $b = 2\pi f_{begin}$. The variables f_{begin} and f_{end} are the beginning and ending frequency (Hz), respectively, and n is the number of data points in the generated waveform. The waveform was generated at a digital sampling rate of 2 megasamples/s and applied at the counter electrode. As a consequence, all of the frequencies in a desired range (in our case, 10 Hz to 300 kHz) can be applied in a very short time frame (2 s).

The current response at each potential (i.e., the formal potential of the SAM and the background potential) was collected and amplified using a locally constructed broadband current amplifier having a 3 db point of 1.5 MHz. The data were digitized at the same sampling rate as generated and then Fourier transformed to yield the current-frequency curves. The signal generation, data collection, and signal processing were all performed using a routine written in LabVIEW 6i (National Instruments, Austin, TX).

The Fourier transformed data obtained in the SWAV experiment were analyzed in the same manner as described above, that is, a plot of I_{peak}/I_{bkgd} versus frequency was generated and fit to a Randles equivalent circuit.[24,26] In this model, the circuit elements, C_{dl}, C_{ads}, and R_{ct}, are related to the SAM parameters via the following equations:

$$C_{dl} = (C/A)(A) \quad (2)$$

$$C_{ads} = (F^2A\Gamma)/(4RT) \quad (3)$$

$$R_{ct} = (2RT)/(F^2A\Gamma k_{et}) \quad (4)$$

where C/A is the double-layer capacitance per unit area, A is the electrode area, Γ is the number of redox-active species per unit area, k_{et} is the electron-transfer rate constant, and the other constants have their usual meaning. Rearrangement of these equations yields

$$k_{et} = 1/(2R_{ct}C_{ads}) \quad (5)$$

The value of k_{et} (which equals k^0 when the applied potential equals the formal potential) is determined from the experimental curves by using a spreadsheet program (Excel, Microsoft, Redmond WA; obtained from S. E. Creager) by adjusting the two (for the most part) independent parameters R_{ct} and C_{ads}. This program also permits the modeling of dispersive kinetics.[26] As has been detailed by Creager and co-workers, the fitting routine is considerably less technical and more readily interpretable than other nonlinear least-squares fitting routines typically employed to fit impedance-type data.[24,26] Owing to the large number of data points in the SWAV data sets, the Fourier transformed data were boxcar averaged to reduce the number of points to a manageable number prior to entering them into the spreadsheet program.

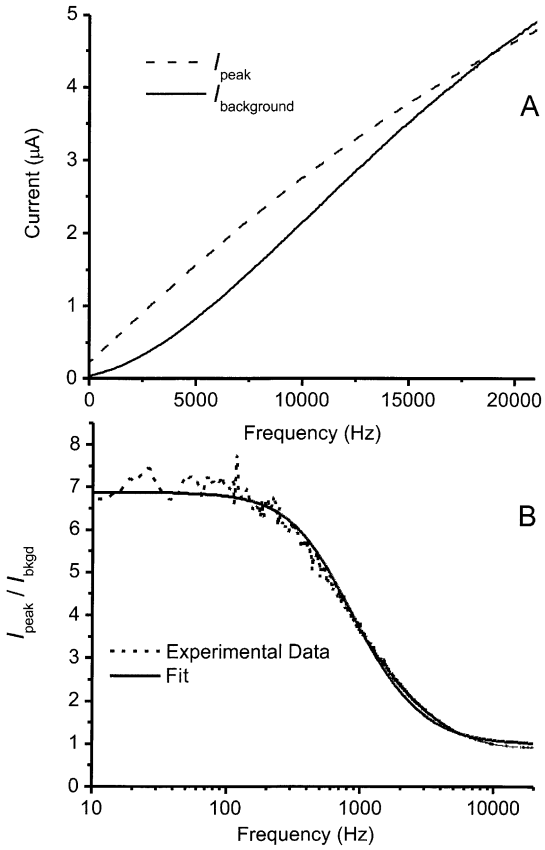

Figure 2. Swept-waveform AC voltammetry (SWAV) for a ferrocene SAM derived from $Fc(CH_2)_{12}SH$ and $CH_3(CH_2)_{11}SH$ in 1:9 ratio. (A) Frequency response (10−20 000 Hz) with a DC offset equal to the formal potential of 0.23 V (top line, I_{peak}) and at a background potential of 0 V (bottom line, I_{bkgd}). (B) Ratio of I_{peak}/I_{bkgd} versus frequency. The solid line represents a fit to the data using a Randles equivalent circuit. The fitting parameters are $k^0 \sim 1900\ s^{-1}$ and $\Gamma \sim 2.4 \times 10^{-11}$ mol cm^{-2}. The k^0 value is in good agreement with a value of 1800 s^{-1} found previously under very similar conditions of surface coverage, solvent, and electrolyte.[27]

Prior to using the SWAV method for examining the redox kinetics of the porphyrin SAMs, the efficacy of the technique was tested on the ferrocene SAM (prepared from $Fc(CH_2)_{12}SH$ and $CH_3(CH_2)_{11}SH$ in 1:9 ratio), for which k^0 has been previously determined to be $\sim$1800 s^{-1}.[27] The SWAV data obtained for this SAM are shown in Figure 2. Figure 2A shows the observed current as a function of frequency for applied potentials at the formal potential (0.23 V) of the SAM and at a background potential (0 V). The two curves were generated by Fourier transforming the raw SWAV data (not shown). Figure 2B shows a plot of I_{peak}/I_{bkgd} versus frequency (log scale) along with a fit to the data generated using the Randles equivalent circuit. This fit yields a value of $k^0 \sim 1900\ s^{-1}$, which is in good agreement with the previously determined value of $\sim$1800 s^{-1}.[27]

The SWAV experiments on the ferrocene SAM demonstrate that this method can be used effectively to obtain standard electron-transfer rate constants. The SWAV method has certain advantages over the frequency domain method. (1) The short time frame of the experiment ensures accurate application of the offset potential because the reference electrode is stable on the time scale of the measurement. (2) The analysis time is very short allowing for easy multiplexing. (3) The data collection

and processing is simple and can be completed "online" immediately after the data are digitized. These advantages, combined with the fact that the ratiometric method permits data analysis in a spreadsheet using only two adjustable parameters, make the SWAV method particularly attractive for measuring the redox kinetics of SAMs.

Determination of Charge-Retention Times. The charge-retention times of the porphyrin SAMs were measured using open circuit potential amperometry (OCPA) as we have previously described.[1−4] Initially, the SAM is oxidized with a 20-ms (much greater than the RC time constant of the cell) pulse that is ∼100 mV above the formal potential of the desired redox state. The applied potential is disconnected from the counter electrode for a period of time that is varied to probe the kinetics of charge recombination in the absence of an applied field. During the disconnect time, two events take place: (1) The electrochemical cell relaxes to the open circuit potential (OCP). (2) The applied potential is changed to match the empirically determined OCP. The counter electrode is then reconnected, at which time the SAM is reduced (because the OCP is at a reducing potential), and the resulting current is monitored. The magnitude of the observed current is directly proportional to the number of molecules that remain oxidized on the surface while the counter electrode is disconnected. A dramatic reduction in charging current results from the fact that the electrochemical cell is already poised at the OCP before reconnection of the counter electrode. Charge retention is measured by successively changing the disconnect time up to a point where essentially all of the molecules that were initially oxidized have decayed back to the neutral state.

Results

Voltammetric Characteristics of the Porphyrin SAMs. Representative fast-scan (100 V s^{-1}) cyclic voltammograms for the porphyrin SAMs are shown in Figure 3. The voltammograms shown are for the **PEP** SAM (panel A) and **TD** SAM (panel B). We have previously reported fast-scan voltammetry for several porphyrin SAMs, including all the molecules shown in Figure 1.[1−10] The voltammograms for the SAMs of the other monomeric porphyrins shown in the figure are similar to those of the **PEP** SAM. Likewise, the voltammograms of other triple-decker SAMs are similar to that of the **TD** SAM studied herein. The voltammograms of the monomeric porphyrin SAMs are characterized by two waves that correspond to the mono- and dication radicals. The voltammograms of the triple-deckers typically exhibit four waves that correspond to the mono-, di-, tri-, and tetracations. The voltammograms shown in Figure 3 were recorded using CH_2Cl_2 as the solvent. The voltammograms observed using ethanol (which has a higher dielectric constant) or propylene carbonate (which has a much higher dielectric constant and is more viscous) as the solvent are very similar, although the detailed characteristics of the voltammetric waves (redox potentials, peak widths, etc.) are somewhat different from those observed in CH_2Cl_2.

There are several noteworthy features in the voltammograms of the porphyrin SAMs. These features are as follows.

(1) As we have previously reported, the redox potentials ($E_{1/2}$) for the porphyrin SAMs are more positive than those observed for the same porphyrin in solution.[1−10] Moreover, the magnitude of the positive potential shift for the SAM depends on the surface coverage (Γ). For example, the potentials for **PEP** (and the other monomeric porphyrins) in solution are $E_{1/2}{}^{0/+1} \sim 0.58$ V and $E_{1/2}{}^{+1/+2} \sim 0.86$ V.[5] The potentials for the **PEP** SAM at low surface coverage ($\Gamma \sim 3.4 \times 10^{-12}$ mol cm^{-2}) are $E_{1/2}{}^{0/+1}$ ~ 0.70 V and $E_{1/2}{}^{+1/+2} \sim 1.01$ V. At higher surface coverage ($\Gamma \sim 2.6 \times 10^{-11}$ mol cm^{-2}) the values are $E_{1/2}{}^{0/+1} \sim 0.78$ V and $E_{1/2}{}^{+1/+2} \sim 1.10$ V. This trend continues as the surface coverage increases further. Similar behavior is observed for the **TD** (and other triple-decker) SAMs versus the **TD** in solution. In particular, the potentials for **TD** in solution are $E_{1/2}{}^{0/+1} \sim 0.16$ V, $E_{1/2}{}^{+1/+2} \sim 0.61$, $E_{1/2}{}^{+2/+3} \sim 1.01$ V, and $E_{1/2}{}^{+3/+4} \sim 1.31$.[3] For the **TD** SAM at $\Gamma \sim 1.3 \times 10^{-11}$ mol cm^{-2}, the potentials are $E_{1/2}{}^{0/+1} \sim 0.29$ V, $E_{1/2}{}^{+1/+2} \sim 0.74$, $E_{1/2}{}^{+2/+3} \sim 1.16$ V, and $E_{1/2}{}^{+3/+4} \sim 1.43$. As is the case for the monomeric porphyrin SAMs, the potentials for the triple-decker SAMs shift even more positively as the surface coverage increases further. For both the monomeric porphyrin SAMs and the triple-decker SAMs, the maximum potential shifts in the SAM versus solution are ∼0.25 V. The shifts appear to be limited only because a maximum surface coverage has been reached.

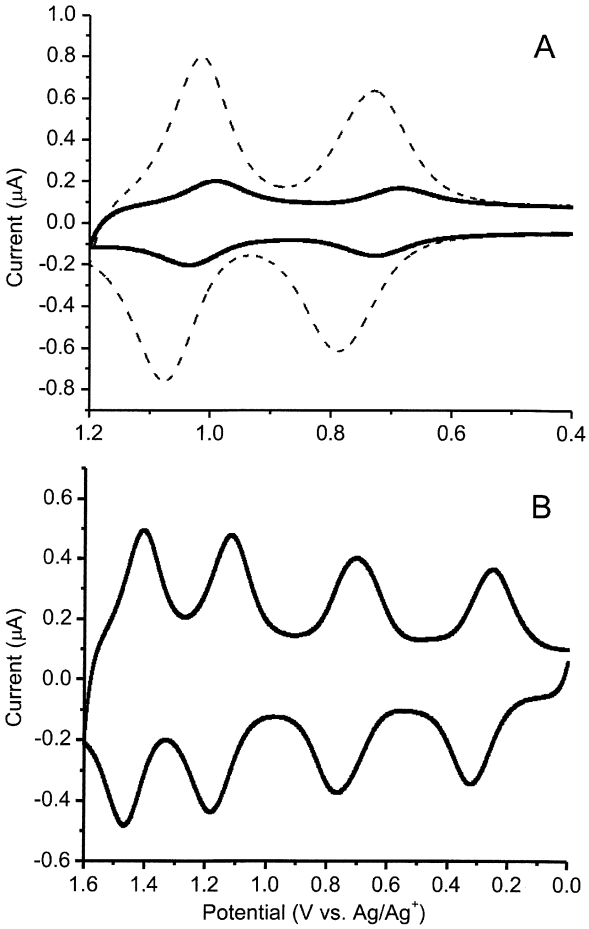

Figure 3. Representative fast-scan (100 V s^{-1}) cyclic voltammograms of the SAMs in CH_2Cl_2/1 M Bu_4NPF_6. (A) **PEP** SAM: (solid line) $\Gamma \sim 3.4 \times 10^{-12}$ mol cm^{-2}; $E_{1/2}{}^{0/+1} \sim 0.70$ V; $E_{1/2}{}^{+1/+2} \sim 1.01$ V. (dashed line) $\Gamma \sim 2.6 \times 10^{-11}$ mol cm^{-2}; $E_{1/2}{}^{0/+1} \sim 0.78$ V; $E_{1/2}{}^{+1/+2} \sim 1.10$ V. (B) **TD** SAM: $\Gamma \sim 1.7 \times 10^{-11}$ mol cm^{-2}; $E_{1/2}{}^{0/+1} \sim 0.29$ V; $E_{1/2}{}^{+1/+2} \sim 0.74$ V; $E_{1/2}{}^{+2/+3} \sim 1.16$ V; $E_{1/2}{}^{+3/+4} \sim 1.43$ V.

(2) For all the porphyrin SAMs, the anodic and cathodic peak maxima (ΔE_{pp}) are split. The value of ΔE_{pp} varies with surface coverage as does the full width at half-maximum of the peak (E_{fwhm}). For example, for the **PEP** SAM at low surface coverage, $\Delta E_{pp} \sim 35$ mV and $E_{fwhm} \sim 95$ mV. At higher surface coverage, $\Delta E_{pp} \sim 50$ mV and $E_{fwhm} \sim 110$ mV. Qualitatively similar trends are observed for the **TD** SAM. However, the values for ΔE_{pp} and E_{fwhm} for the **TD** SAM are intrinsically larger than those of the monomeric porphyrin SAMs (e.g., for the **TD** SAM at $\Gamma \sim 1.3 \times 10^{-11}$ mol cm^{-2}, $\Delta E_{pp} \sim 75$ mV and $E_{fwhm} \sim 150$ mV) and the changes in these parameters with surface coverage

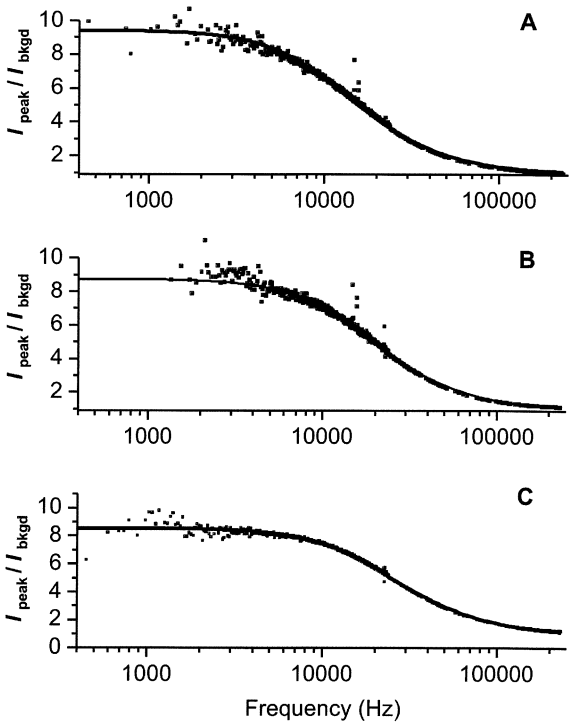

Figure 4. I_{peak}/I_{bkgd} (dotted lines) versus frequency for the phenylmethylene-linked porphyrin SAMs. The solid lines represent fits to the data using a Randles equivalent circuit. The fitting parameters are as follows: (A) **PM3** SAM: $k^0 \sim 4.1 \times 10^4$ s^{-1}; $\Gamma \sim 1.4 \times 10^{-11}$ mol cm^{-2}. (B) **PM2** SAM: $k^0 \sim 4.9 \times 10^4$ s^{-1}; $\Gamma \sim 1.1 \times 10^{-11}$ mol cm^{-2}. (C) **PM1** SAM: $k^0 \sim 5.9 \times 10^4$ s^{-1}; $\Gamma \sim 1.3 \times 10^{-11}$ mol cm^{-2}.

appear less pronounced. Finally, the values of ΔE_{pp} and E_{fwhm} do not change as a function of scan rate in the range accessible to our equipment (300 V s^{-1} and less).

Electron-Transfer Characteristics of the Porphyrin SAMs. Representative plots of I_{peak}/I_{bkgd} for the phenylmethylene-linked porphyrin SAMs, the ethynylphenyl-linked porphyrin SAMs, and the **TD** SAM are shown in Figures 4−6, respectively. In Figure 4, the data for **PM0** are omitted for clarity. In the monomeric porphyrin SAMs, the electron-transfer kinetics were examined only for the monocations. The data for I_{peak} and I_{bkgd} were obtained at $E_{1/2}{}^{0+/1}$ and 0 V, respectively. For the **TD** SAM, the electron-transfer kinetics were examined for each of the four cationic oxidation states. The data for I_{peak} were obtained at $E_{1/2}{}^{+n/+(n+1)}$; the data for I_{bkgd} for the monocation were obtained at 0 V, whereas those for the di-, tri-, and tetracations were obtained at a potential 150 mV below $E_{1/2}{}^{+n/+(n+1)}$. The k^0 values obtained from fits of the I_{peak}/I_{bkgd} plots shown in Figures 4−6 are summarized in Table 1. The effect of surface coverage on the electron-transfer kinetics was also investigated for the phenylmethylene-linked porphyrin SAMs and the **TD** SAM. The k^0 values obtained at different surface coverages for these SAMs are also included in Table 1. Small variations in the fitting parameters for the I_{peak}/I_{bkgd} plots give equally good fits to the data. These variations alter the k^0 values by ±10%. Selected measurements using propylene carbonate/Bu_4NPF_6 or ethanol/Bu_4NClO_4 as the solvent/electrolyte resulted in k^0 values that differed somewhat from those observed using CH_2Cl_2/Bu_4NPF_6. However, the differences in rates were generally small (∼10%) and approached the uncertainty in the k^0 values.

Inspection of the kinetic data for the porphyrin SAMs reveals the following noteworthy features.

(1) The electron-transfer rates for the phenylmethylene-linked porphyrin SAMs are generally less than those of the ethynylphenyl-linked porphyrin SAMs. For the former class of SAMs, the k^0 values range from ∼2.5×10^4 s^{-1} to ∼7.5×10^4 s^{-1}. For the latter class of SAMs, the k^0 values range from ∼7.5×10^4 s^{-1} to ∼15×10^4 s^{-1}. The rates for both types of monomeric porphyrin SAMs monotonically decrease as the length of the linker increases. The electron-transfer rates for the **TD** SAM are generally less than those of either the phenylmethylene-linked porphyrin SAMs or the ethynylphenyl-linked porphyrin SAMs; the k^0 values for the **TD** SAM range from ∼2.5×10^4 s^{-1} to ∼4.5×10^4 s^{-1}. In addition, the k^0 values for the **TD** SAM decrease monotonically as the oxidation state increases.

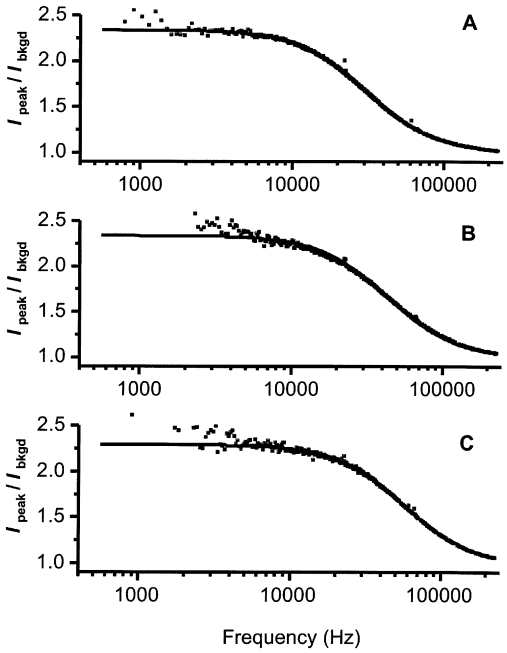

Figure 5. I_{peak}/I_{bkgd} (dotted lines) versus frequency for the ethynylphenyl-linked porphyrin SAMs. The solid lines represent fits to the data using a Randles equivalent circuit. The fitting parameters are as follows: (A) **PEPM** SAM: $k^0 \sim 7.5 \times 10^4$ s^{-1}; $\Gamma \sim 0.52 \times 10^{-11}$ mol cm^{-2}. (B) **PEP** SAM: $k^0 \sim 11 \times 10^4$ s^{-1}; $\Gamma \sim 0.61 \times 10^{-11}$ mol cm^{-2}. (C) **EP** SAM: $k^0 \sim 15 \times 10^4$ s^{-1}; $\Gamma \sim 0.84 \times 10^{-11}$ mol cm^{-2}.

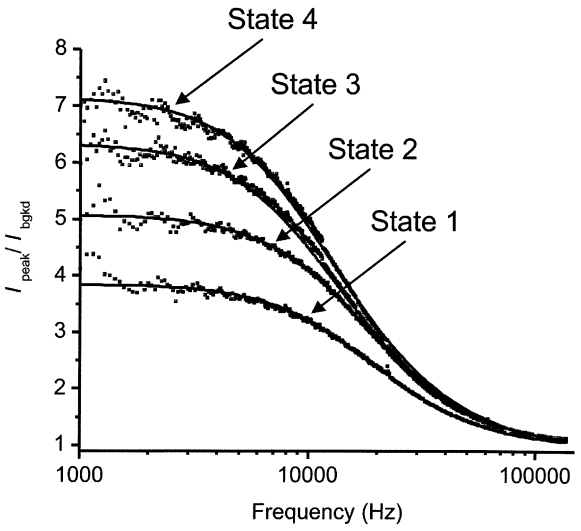

Figure 6. I_{peak}/I_{bkgd} (dotted lines) versus frequency for the mono-, di-, tri-, and tetracations (states 1−4, respectively) of the **TD** SAM. The solid lines represent fits to the data using a Randles equivalent circuit. The fitting parameters are as follows: $\Gamma \sim 0.22 \times 10^{-11}$ mol cm^{-2}. State 1, $k^0 \sim 4.5 \times 10^4$ s^{-1}; State 2, $k^0 \sim 4.1 \times 10^4$ s^{-1}; State 3, $k^0 \sim 3.0 \times 10^4$ s^{-1}; State 4, $k^0 \sim 2.8 \times 10^4$ s^{-1}.

TABLE 1: Comparison of Electron-Transfer Rates (k^0) and Charge-Retention Times ($t_{1/2}$) for the SAMs[a]

molecule	Γ (x10^{-11} mol cm^{-2})	k^0 (x10^4 s^{-1})	$t_{1/2}$ (s)
Porphyrins with Phenylmethylene Linkers			
PM0	0.74	7.5	28
	0.84	4.5	76
PM1	1.3	5.9	57
	1.7	5.3	82
	4.6	2.4	120
PM2	1.1	4.9	220
	1.2	3.7	*b*
PM3	1.4	4.1	430
	1.8	2.6	*b*
Porphyrins with Ethynylphenyl-Derived Linkers			
EP	0.84	15	21
PEP	0.61	11	23
PEPM	0.52	7.5	59
TD (Phenylethynylphenyl Linker)			
state1	0.22	4.5	11
	0.80	3.5	45
state 2	0.22	4.1	25
	0.80	3.4	120
state 3	0.22	3.0	34
	0.80	3.0	140
state 4	0.22	2.8	49
	0.80	2.6	170

[a] Alterations in the fitting parameters for the SWAV and OCPA data that give equally good fits change the k^0 and $t_{1/2}$ values by ±10%. [b] Not determined.

(2) The electron-transfer rates depend on the surface coverage of the SAM. In all cases, the k^0 values decrease as the surface coverage increases. The effects of surface coverage on the rates can overshadow the effects of linker length. For example, the electron-transfer rate for **PM3** (three methylene spacers in the linker) at $\Gamma \sim 1.4 \times 10^{-11}$ mol cm^{-2} is $k^0 \sim 4.1 \times 10^4$ s^{-1}. This rate is faster than that exhibited by **PM1** (one methylene spacer in the linker) at the higher surface coverage of $\Gamma \sim 4.6 \times 10^{-11}$ mol cm^{-2}, for which $k^0 \sim 2.4 \times 10^4$ s^{-1}.

To further investigate the effects of surface coverage on the electron-transfer rates, a detailed study was undertaken on the **PM1** SAM. During this study, the electron-transfer kinetics were measured at 16 different surface coverages ranging from $\Gamma \sim 1 \times 10^{-11}$ mol cm^{-2} to $\Gamma \sim 1 \times 10^{-10}$ mol cm^{-2}. The results of this study are shown in Figure 7. At low surface coverages ($\Gamma < 3 \times 10^{-11}$ mol cm^{-2}), the k^0 values decrease monotonically as the surface coverage increases. At higher surface coverages, the rates appear to converge to a nearly constant value, with $k^0 \sim 2 \times 10^4$ s^{-1}. In the range of coverages investigated, the k^0 value varies by approximately a factor of 4.

Finally, at high surface coverages, the quality of the fits to the I_{peak}/I_{bkgd} plots were not as good as those at lower coverage. The concentration at which the quality of the fits begins to degrade depends on the type of molecule in the SAM. In the ethynylphenyl-linked porphyrin SAMs, satisfactory fits could not be obtained when the coverages exceeded $\Gamma \sim 1 \times 10^{-11}$ mol cm^{-2}. Hence, only data obtained at relatively low coverage are given for these molecules in Table 1. In contrast, good fits could be obtained for the phenylmethylene-linked porphyrin SAMs at surface concentrations approaching nearly 10-fold larger. The **PM0** SAM is the exception; good fits could only be obtained for this SAM at much lower surface concentrations. We attempted to fit the data which failed to fit the homogeneous kinetic model using the dispersive kinetic model that is included in the spreadsheet fitting program.[26] However, no satisfactory fits could be obtained, even by including up to 10 rate constants.

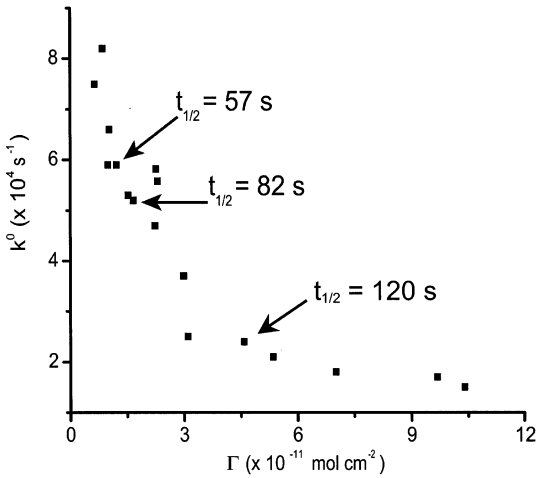

Figure 7. Plot of k^0 (squares) versus Γ for the **PM1** SAM. The charge-retention half-lives ($t_{1/2}$) observed at selected Γ values are also indicated. The values at these points are as follows: $t_{1/2} \sim 57$ s; $k^0 \sim 5.9 \times 10^4$ s^{-1}, $\Gamma \sim 1.3 \times 10^{-11}$ mol cm^{-2}. $t_{1/2} \sim 82$ s; $k^0 \sim 5.3 \times 10^4$ s^{-1}, $\Gamma \sim 1.5 \times 10^{-11}$ mol cm^{-2}. $t_{1/2} \sim 120$ s; $k^0 \sim 2.4 \times 10^4$ s^{-1}, $\Gamma \sim 4.6 \times 10^{-11}$ mol cm^{-2}.

Charge-Retention Characteristics of the Porphyrin SAMs. The charge-retention characteristics of the porphyrin SAMs were investigated in parallel with the redox kinetics. The $t_{1/2}$ values for charge retention for the various SAMs are included in Table 1. Alteration of the fitting parameters for the OCPA data to give equally good fits changes the $t_{1/2}$ values by ±10%. As was the case for the redox-kinetic studies described above, selected charge-retention measurements were made using propylene carbonate/Bu_4NPF_6 and ethanol/Bu_4NClO_4 as the solvent/electrolyte rather than CH_2Cl_2/Bu_4NPF_6. As is the case for the k^0 values, the $t_{1/2}$ values measured in these solvent/electrolye systems were somewhat different than those measured in CH_2Cl_2/Bu_4NPF_6; however, the differences in $t_{1/2}$ values are small (∼10%) and approach the uncertainty in $t_{1/2}$ values.

Even though the charge-retention characteristics were not as extensively examined as the redox kinetics, certain trends are apparent in the data. In particular, as is the case for the electron-transfer rates, the charge-retention times depend on the surface coverage of the SAM. At low surface coverages, the $t_{1/2}$ values increase monotonically as the surface coverage increases. This trend is illustrated by the data obtained for the **PM1** SAM for which $t_{1/2} \sim 57$, 82, and 120 s for $\Gamma = 1.3$, 1.7, and 4.6 (x10^{-11} mol cm^{-2}), respectively. To further illustrate this trend, these data points are highlighted in Figure 7. Together, the kinetic- and charge-retention data indicate that the rate of electron transfer in the presence of applied potential and the rate of charge dissipation in the absence of applied potential both decrease as the porphyrin molecules in the SAMs become more densely packed. This general trend encompasses all of the linker types and architectures investigated.

Discussion

The electrochemical, redox-kinetic, and charge-retention data obtained for the porphyrin SAMs provide a foundation for attaining a self-consistent view of these monolayers. The SAMs were prepared from a library of porphyrinic molecules that vary in the composition and length of the linker attached to the surface as well as the nature of the redox-active moiety (porphyrin monomer versus triple decker). One theme that emerges is that the rate of electron transfer in the presence of applied potential and the rate of charge dissipation in the absence of applied potential are directly correlated, that is, SAMs with

faster electron-transfer rates exhibit faster charge dissipation (shorter charge retention) and vice versa. This behavior is arguably not surprising given that both processes involve the transfer of charge between the redox center and the Au electrode. What is perhaps more remarkable is that the correlation holds although the time scales for the two processes differ by approximately 6 orders of magnitude. Another theme that emerges is that the electron-transfer and charge-dissipation rates are affected by the packing density of the molecules in the SAM. The rates for both of these processes slow as the SAMs become more densely packed. In general, the electron-transfer and charge-dissipation rates can be altered 3- to 4-fold by varying the surface coverage. While the variations in rate due to changes in surface coverage are not extremely large, they can potentially blur any systematic trends in rate observed for molecules with different linker lengths/types.

In the sections below, we will discuss the electron-transfer and charge-retention characteristics of the porphyrin SAMs in more detail. First, we address the issue of how the linker and porphyrin architecture affect these characteristics. Next, we address the effects of surface coverage and the related issue of monolayer homogeneity. Finally, we discuss the large disparities in the time scales of electron transfer (applied potential) versus charge dissipation (no applied potential).

Effects of Linker and Porphyrin Architecture on Electron-Transfer and Charge-Retention Characteristics. As was noted in the Introduction, our previous studies of the charge-retention characteristics of porphyrin SAMs have revealed certain qualitative trends. In particular, (1) SAMs of porphyrins with nonconjugated linkers generally exhibit longer charge-retention times than those with conjugated linkers and (2) the extension of the linker by the addition of methylene groups increases the charge-retention time.[1,2] The studies reported herein show that trends in the electron-transfer kinetics as a function of linker type parallel those for charge retention (see Table 1). We stress, however, that these trends are qualitative at best and that there are anomalies.

Previous studies of electron-transfer processes in redox-active SAMs have shown that the rates typically fall off exponentially with the distance of the redox center from the electroactive surface ($k \propto \exp(-\beta R_e)$, where β is a constant). The value of β depends on the nature of the linker and is $\sim$1.0 per $-CH_2-$ group and considerably smaller for conjugated linkers.[11−16,21,22,28,32] The body of data available for the porphyrin SAMs is not sufficient to develop a meaningful quantitative distance−rate relationship. Indeed, we emphasize that this aspect of the electron-transfer properties of the porphyrin SAMs is not the objective of the present work. Moreover, there are several important differences between the porphyrin SAMs studied herein versus other types of redox-active SAMs that have been typically investigated. These include the following.

(1) The linkers for the porphyrin SAMs are relatively short and the total variation in length from shortest (**PM0**; phenyl ring, $\sim$6 Å) to longest (**PEPM**; phenylethynylphenyl-methylene, $\sim$12 Å) is relatively small ($\sim$6 Å). In contrast, studies of alkyl- and aryl-linked ferrocenes have typically involved much longer linkers or much larger variations in linker length.[11−14,21,28] The use of long linkers (and larger linker-length variation) minimizes artifacts that could compromise rate−distance relationships.

(2) The porphyrin SAMs contain no diluents; consequently, the surface coverage is relatively sparse for the SAMs with lower surface concentration. For example, $\Gamma \sim 10^{-11}$ mol cm^{-2} corresponds to a molecular area of $\sim$525 Å^2. This area is much larger than that occupied by a porphyrin molecule in a tightly packed monolayer ($<$100 Å^2/ molecule).[1,33,34] In contrast, studies aimed at developing rate−distance relationships employed SAMs wherein the electrode surface is completely covered (redox molecule plus diluent). Complete coverage also precludes effects that would compromise rate−distance relationships, such as conformational changes that would allow access of the redox-active component to the surface, thereby facilitating direct charge recombination to the surface (although such processes do not appear to be operative in the porphyrin SAMs (vide infra)). The formation of domains (via clustering of molecules) is not consistent with the systematic variation in k^0, $E_{1/2}$, and $t_{1/2}$ values observed with variation in surface coverage.

One noteworthy characteristic of the redox kinetics exhibited by all the porphyrin SAMs regardless of linker type/length is that the electron-transfer rates are generally slower than those observed for other redox-active species tethered with similar linkers or at similar distances from the Au surface.[12,14,18] For example, the **EP** SAM has a single ethynylphenyl linker and gives $k^0 \sim 1.5 \times 10^5$ s^{-1} ($\Gamma \sim 6.0 \times 10^{-12}$ mol cm^{-2}), whereas a dilute ferrocene SAM tethered by a linker with three ethynylphenyl groups has $k^0 \sim 5 \times 10^5$ s^{-1}.[21] The fact that the electron-transfer rate for the porphyrin SAMs is less than that expected suggests that the sparse surface coverage of these SAMs is not a significant factor in governing the rates. In particular, sparse coverage could allow the porphyrins to tilt with respect to the surface normal, thereby bringing the redox center closer to the surface than is possible in a more densely packed monolyer. A tilted orientation could in turn promote direct charge recombination from the redox center to the surface. This type of effect would increase the electron-transfer rates relative to those expected on the basis of linker length/type. Yet the rates of electron transfer for even the most sparsely covered porphyrin SAMs are slower than those expected for a particular linker type.

One plausible explanation for the slower than expected electron-transfer rates of the porphyrin SAMs is that the redox center is intrinsically shielded from solvent/counterions (thereby affecting the reorganization energy), owing to the "self-insulating" character imparted by the bulky, nonpolar, nonlinking substituent groups. SAM formation in general partially shields the redox centers from solvent/counterions, as is evidenced by the positive shift in $E_{1/2}$ values in SAMs versus solution.[3,5−10,35−37] Furthermore, previous studies of alkylferrocene SAMs have shown that when the redox center is buried within an insulating matrix of longer alkane chains, the redox kinetics are dramatically slower.[23,27] Related studies in which large polymeric counterions are employed yield similar results.[23,27] Indeed, the combination of these two factors can render a redox-active SAM completely electro-inactive.[38] Solvent/counterion exclusion also strongly attenuates the rate−distance behavior of the redox kinetics of SAMs.[16]

Finally, the detailed characteristics of electron transfer could be affected by the charge density in the counteranion (and therefore on the type of anion) or on the dielectric property of the solvent (slower electron-transfer rates are typically observed in solvents with low dielectric constants, which, therefore, have longer longitudinal relaxation times[39]). However, the electron-transfer characteristics of the porphyrin SAMs do not appear to be strongly dependent on these properties (as evidenced by the fact that the electron-transfer rates in different solvent/counterion systems are qualitatively similar). At the highest surface coverages, space charge effects may also modulate the electron-transfer rates of the porphyrin SAMs. This issue will be discussed further in the next section.

Effects of Surface Coverage and Monolayer Homogeneity on Electron-Transfer and Charge-Retention Characteristics. The observation that both the electron-transfer and charge-dissipation rates slow as the surface concentration of the porphyrin SAMs increases is generally consistent with the notion that solvent/counterion screening and the accompanying effect on reorganization energy is a key factor in controlling the rates of both processes. In particular, the more densely packed the SAM becomes, the more restricted is the access of the solvent/counterions from the redox center. The incomplete compensation of positive charge on the redox centers leads to space-charge effects that modulate the electron-transfer behavior. The fact that the $E_{1/2}$ values shift to progressively more positive potentials as the surface concentration increases is further consistent with this general view.[31]

A secondary effect of increasing the surface coverage in the porphyrin SAM is that the redox behavior becomes more heterogeneous. This thermodynamic heterogeneity (distribution of formal potentials) is evidenced by the fact that the E_{fwhm} of the voltammetric peaks for the porphyrin SAMs increases as the surface concentration increases. For example, the **PEP** SAM exhibits an E_{fwhm} of ~95 mV at low surface coverage ($\Gamma \sim 3.4 \times 10^{-12}$ mol cm^{-2}). This value is near the ideal value of $E_{fwhm} \sim 90$ mV/n expected for a homogeneous SAM.[31,40] Increasing the surface coverage approximately 8-fold ($\Gamma \sim 2.6 \times 10^{-11}$ mol cm^{-2}) results in an $E_{fwhm} \sim 110$ mV, which is in a range where a distribution of formal potentials exists.[15] In the **TD** SAM, the monolayers appear to be intrinsically more heterogeneous than those of the monomeric porphyrins. This is evidenced by the generally larger E_{fwhm} at comparable surface coverages. The thermodynamic heterogeneity exhibited by the porphyrin SAMs at higher surface coverages could arise either from a distribution in the conformation/structure of the molecules or from a distribution in the space charge. Indeed, these two effects are most likely interdependent. The more heterogeneous nature of the **TD** SAMs is plausibly because these molecules are much larger, are not symmetrical about the linker axis, and pack more poorly than the monomeric porphyrin SAMs.

The thermodynamic heterogeneity observed for the porphyrin SAMs at high surface coverage implies some level of kinetic dispersion. Kinetic dispersion is difficult to identify using potential step methods[22] but is easily detected using the ratiometric technique used herein.[21,24,26−28] Interestingly, the data for all the porphyrin SAMs can be reasonably well fit using a single k^0 value, even at surface concentrations that give rise to broadening of the voltammetric peaks. These results suggest that the dispersion in the k^0 values is less than the ±10% limit set by the fitting procedure. More interestingly, the Randles equivalent circuit model fails at very high surface concentrations. This failure occurs without passing though a regime wherein a dispersive kinetic model does account for the data. The rationale for this behavior is not certain but may lie in certain assumptions in the fitting procedure. We will return to this issue below.

Another noteworthy feature of the voltammetric data for all the porphyrin SAMs is that the anodic and cathodic peaks are intrinsically split and that this splitting varies with surface coverage. In an ideal SAM, ΔE_{pp} should be zero.[31,40] The nonzero value of ΔE_{pp} for the porphyrin SAMs is not due to kinetic effects, as is evidenced by the fact that the splitting is independent of scan rate and persists at very low scan rates. In this regard, Amatore and co-workers have observed similar effects in the voltammetric behavior of immobilized redox-active dendrimers.[41] These workers ascribed the nonzero ΔE_{pp} values to a difference in free energies for the oxidative and reductive process (thereby leading to different potentials). In essence, the molecules undergo a phase transition upon alteration of redox state. In the porphyrin SAMs, such a phase transition could arise because there is some degree of electronic interaction between the redox centers (i.e., the self-insulating property of the molecules is not perfect). The fact that the ΔE_{pp} values increase with increasing surface coverage is further consistent with this notion.

The fact that ΔE_{pp} is nonzero for the porphyrin SAMs could come into play in the fitting of the kinetic data and in particular explain why a dispersive model never appears to fit the data. An assumption in the model is that the I_{peak} values are acquired at the formal potential. For practical reasons, we have taken this value to be $E_{1/2}$. When the distribution of formal potentials is small, the fact that the $E_{1/2}$ value is not actually equal to the formal potential of a subset of the molecules has little impact on the fits. On the other hand, as the distribution of formal potentials becomes broader, the $E_{1/2}$ value is less representative of the formal potential for the different domains in the heterogeneous SAM. Thus, for domains in which the formal potential is the furthest from the $E_{1/2}$ value, the measurement is made at nonnegligible over/underpotential. This violates the assumption of the modeling procedure. This view would indicate that a dispersive kinetic picture is still appropriate at higher surface concentrations. However, the current model cannot be readily applied in situations when the free energies for the oxidative and reductive processes are different.

Relationship of Electron-Transfer and Charge-Dissipation Rates. A final noteworthy characteristic of the porphyrin SAMs is that the electron-transfer rates in the presence of applied potential differ from the charge-dissipation rates in the absence of applied potential by nearly 6 orders of magnitude. A rigorous explanation for this behavior requires additional studies including theoretical modeling that accurately accounts for the electronic structure of the surface/SAM architecture. Regardless, the fact that these rates are so different indicates that the tunneling behavior of the electron through the linker barrier is radically different in the presence versus absence of applied potential. Several factors could affect these rates. These factors could possibly include conformational relaxation both at the individual molecule and bulk monolayer level and solvent/counterion relaxation effects. However, the fact that the large disparity in electron-transfer and charge-dissipation rates persists even for sparse monolayers strongly suggests that bulk effects cannot play the dominant role.

Recent theoretical studies by Brédas and co-workers provide a possible alternative explanation for the disparities in the electron-transfer and charge-dissipation rates.[42] These workers investigated the effects of electric fields on the conductivity of molecules that exhibit negative-differential resistance behavior. The studies showed that the conductivity through insulating spacers (such as $-CH_2-$ groups) was significantly affected by electric-field gradients comparable to those generated in redox experiments on SAMs. A key difference in the conditions under which the electron-transfer and charge-dissipation rates are determined is that the electric-field gradient across the SAM must be significantly different. In particular, the redox experiment is designed such that the electric field falls steeply across the molecules in the SAM.[43] When the applied potential is removed, the electric-field gradient collapses as the electrode polarization relaxes to equilibrium. These large inherent differences in electric-field gradient in the presence versus absence of applied potential could be responsible for the vastly different

electron-tunneling rates through the linker-atom barrier in the porphyrin SAMs.

Conclusions

The studies reported herein delineate the factors that control the electron-transfer (applied potential) and charge-dissipation (no applied potential) characteristics of the porphyrin SAMs. The general theme that emerges is that these rates parallel one another, that is, SAMs that exhibit fast rates of electron transfer also dissipate charge more rapidly. Accordingly, a fundamental trade off exists that has important implications for device applications. In particular, long charge-retention times are highly desirable in most memory applications. The longer the retention times, the less frequent the refresh rates, leading to lower power consumption. On the other hand, many memory applications also require fast read/write/erase times. The studies of the porphyrin SAMs reported herein indicate that the relative magnitudes of the electron-transfer and charge-dissipation rates can be manipulated to some extent via molecular design considerations. The exact choice of molecules for use in a particular device will depend on the nature of the operational features desired in the device balanced by the fundamental limitations in the relative magnitude of the electron-transfer versus charge-dissipation rates. In this respect, the ability to design and synthesize a wide variety of redox-active molecules bearing a linker of choice augurs well for tuning the physical properties as needed to meet the criteria for information-storage applications.

Acknowledgment. This work was supported by the DARPA Moletronics Program (MDA972-01-C-0072) and by ZettaCore, Inc. We thank C. Amatore, S. E. Creager, and R. L. McCreery for helpful discussions. We also thank S. E. Creager for making available the spreadsheet program for fitting the ratiometric data.

References and Notes

(1) Roth, K. M.; Dontha, N.; Dabke, R. B.; Gryko, D. T.; Clausen, C.; Lindsey, J. S.; Bocian, D. F.; Kuhr, W. G. *J. Vac. Sci. Technol., B* **2000**, *18*, 2359−2364.

(2) Roth, K. M.; Dabke, R. B.; Liu, Z.; Yasseri, A. A.; Gryko, D. T.; Clausen, C.; Lindsey, J. S.; Bocian, D. F.; Kuhr, W. G. ACS Symposium Series, in press.

(3) Gryko, D.; Li, J.; Diers, J. R.; Roth, K. M.; Bocian, D. F.; Kuhr, W. G.; Lindsey, J. S. *J. Mater. Chem.* **2001**, *11*, 1162−1180.

(4) Roth, K. M.; Lindsey, J. S.; Bocian, D. F.; Kuhr, W. G. *Langmuir* **2002**, *18*, 4030−4040.

(5) Gryko, D. T.; Clausen, C.; Roth, K. M.; Dontha, N.; Bocian, D. F.; Kuhr, W. G.; Lindsey, J. S. *J. Org. Chem.* **2000**, *65*, 7345−7355.

(6) Gryko, D. T.; Zhao, F.; Yasseri, A. A.; Roth, K. M.; Bocian, D. F.; Kuhr, W. G.; Lindsey, J. S. *J. Org. Chem.* **2000**, *65*, 7356−7362.

(7) Clausen, C.; Gryko, D. T.; Dabke, R. B.; Dontha, N.; Bocian, D. F.; Kuhr, W. G.; Lindsey, J. S. *J. Org. Chem.* **2000**, *65*, 7363−7370.

(8) Clausen, C.; Gryko, D. T.; Yasseri, A. A.; Diers, J. R.; Bocian, D. F.; Kuhr, W. G.; Lindsey, J. S. *J. Org. Chem.* **2000**, *65*, 7371−7378.

(9) Li, J.; Gryko, D.; Dabke, R. B.; Diers, J. R.; Bocian, D. F.; Kuhr, W. G.; Lindsey, J. S. *J. Org. Chem.* **2000**, *65*, 7379−7390.

(10) Schweikart, K. H.; Malinovskii, V. L.; Diers, J. R.; Yasseri, A. A.; Bocian, D. F.; Kuhr, W. G.; Lindsey, J. S. *J. Mater. Chem.* **2002**, *12*, 808−828.

(11) Chidsey, C. E. D. *Science* **1991**, *251*, 919−922.

(12) Smalley, J. F.; Feldberg, S. W.; Chidsey, C. E. D.; Linford, M. R.; Newton, M. D.; Liu, Y.-P. *J. Phys. Chem.* **1995**, *99*, 13141−13149.

(13) Sachs, S. B.; Dudek, S. P.; Hsung, R. P.; Sita, L. R.; Smalley, J. F.; Newton, M. D.; Feldberg, S. W.; Chidsey, C. E. D. *J. Am. Chem. Soc.* **1997**, *119*, 10563−10564.

(14) Sikes, H. D.; Smalley, J. F.; Dudek, S. P.; Cook, A. R.; Newton, M. D.; Chidsey, C. E. D.; Feldberg, S. W. *Science* **2001**, *291*, 1519−1523.

(15) Finklea, H. O.; Hanshew, D. D. *J. Am. Chem. Soc.* **1992**, *114*, 3173−3181.

(16) Finklea, H. O.; Liu, L.; Ravenscroft, M. S.; Punturi, S. *J. Phys. Chem.* **1996**, *100*, 18852−18858.

(17) Forster, R. J.; Faulkner, L. R. *J. Am. Chem. Soc.* **1994**, *116*, 5453−5461.

(18) Forster, R. J.; Faulkner, L. R. *J. Am. Chem. Soc.* **1994**, *116*, 5444−5452.

(19) Rowe, G. K.; Creager, S. E. *Langmuir* **1994**, *10*, 1186−1192.

(20) Weber, K.; Hockett, L.; Creager, S. *J. Phys. Chem. B* **1997**, *101*, 8286−8291.

(21) Creager, S.; Yu, C. J.; Bamdad, C.; O'Connor, S.; MacLean, T.; Lam, E.; Chong, Y.; Olsen, G. T.; Luo, J.; Gozin, M.; Kayyem, J. F. *J. Am. Chem. Soc.* **1999**, *121*, 1059−1064.

(22) Carter, M. T.; Rowe, G. K.; Richardson, J. N.; Tender, L. M.; Terrill, R. H.; Murray, R. W. *J. Am. Chem. Soc.* **1995**, *117*, 2896−2899.

(23) Ingram, R. S.; Murray, R. W. *J. Chem. Soc., Faraday Trans.* **1996**, *92*, 3941−3946.

(24) Creager, S. E.; Wooster, T. T. *Anal. Chem.* **1998**, *70*, 4257−4263.

(25) O'Connor, S. D.; Olsen, G. T.; Creager, S. E. *J. Electroanal. Chem.* **1999**, *466*, 197−202.

(26) Li, J.; Schuler, K.; Creager, S. E. *J. Electrochem. Soc.* **2000**, *147*, 4584−4588.

(27) Sumner, J. J.; Creager, S. E. *J. Phys. Chem. B* **2001**, *105*, 8739−8745.

(28) Sumner, J. J.; Weber, K. S.; Hockett, L. A.; Creager, S. E. *J. Phys. Chem. B* **2000**, *104*, 7449−7454.

(29) Chidsey, C. E. D.; Bertozzi, C. R.; Putvinski, T. M.; Mujsce, A. M. *J. Am. Chem. Soc.* **1990**, *112*, 4301−4306.

(30) Tour, J. M.; Jones, L., II; Pearson, D. L.; Lamba, J. J. S.; Burgin, T. P.; Whitesides, G. M.; Allara, D. L.; Parikh, A. N.; Atre, S. *J. Am. Chem. Soc.* **1995**, *117*, 9529−9534.

(31) Bard, A. J.; Faulkner, L. R. *Electrochemical Methods: fundamentals and applications*; Wiley: New York, 2001.

(32) Finklea, H. O. *Electroanal. Chem.* **1996**, *19*, 109−335.

(33) Schick, G. A.; Schreiman, I. C.; Wagner, R. W.; Lindsey, J. S.; Bocian, D. F. *J. Am. Chem. Soc.* **1989**, *111*, 1344−1350.

(34) Van Galen, D. A.; Majda, M. *Anal. Chem.* **1988**, *60*, 1549−1553.

(35) Creager, S. E.; Rowe, G. K. *J. Electroanal. Chem.* **1997**, *420*, 291−299.

(36) Pyati, R.; Murray, R. W. *J. Am. Chem. Soc.* **1996**, *118*, 1743−1749.

(37) Rowe, G. K.; Creager, S. E. *J. Phys. Chem.* **1994**, *98*, 5500−5507.

(38) Campbell, D. J.; Herr, B. R.; Hulteen, J. C.; Van Duyne, R. P.; Mirkin, C. A. *J. Am. Chem. Soc.* **1996**, *118*, 10211−10219.

(39) Yamada, T.; Hashimoto, T.; Kikushima, S.; Ohtsuka, T.; Nango, M. *Langmuir* **2001**, *17*, 4634−4640.

(40) Laviron, E. *J. Electroanal. Chem. Interfacial Electrochem.* **1979**, *101*, 19−28.

(41) Amatore, C.; Bouret, Y.; Maisonhaute, E.; Goldsmith, J. I.; Abruña, H. D. *Chem. Eur. J.* **2001**, *7*, 2206−2226.

(42) Karzazi, Y.; Cornil, J.; Brédas, J. L. *J. Am. Chem. Soc.* **2001**, *123*, 10076−10084.

(43) Smith, C. P.; White, H. S. *Anal. Chem.* **1992**, *64*, 2398−2405.